

Appl. No. 10/516,672
Amdt. dated November 15, 2010

Docket No. 244.1005

EXHIBIT 1

Chapter 1

Introduction

Alumina, also called aluminium oxide, is the only solid oxide of aluminium and has the chemical formula Al_2O_3 . Aluminas, or more precisely, aluminous materials have been technologically significant ceramic materials throughout human history. Before 5000 BC aluminous clays were being used in Mesopotamia for the manufacture of fine pottery. After 3000 BC the Babylonians and Egyptians began employing aluminium compounds in various chemicals, such as perfumes and dyes, and medicines (van Horn *et al.* 2002). Upon these uses the Romans utilised aluminous materials in the manufacture of cosmetics. Emerald, sapphire and ruby, which are crystalline forms of alumina coloured by various impurities, were utilised in jewellery from about 800 BC, no more extensively than during ancient Roman times.

Etymology shows that the word alumina, like the word aluminium, comes from the term *alumen* (Simpson and Weiner 1989), which is Latin for alum (potassium aluminium sulphate, $\text{K}_2\text{SO}_4 \cdot \text{Al}_2(\text{SO}_4)_3 \cdot 12\text{H}_2\text{O}$). The Romans used alum as a styptic or astringent, perfume, and as a mordant in the dyeing process. The earliest extant literature documenting the use and manufacture of alum was by the Roman naturalist Pliny the Elder (*Gaius Plinius Secundus*) in his '*Historia Naturalis*' (77 AD), Books XXXIII & XXXIV). Note that the earliest mention of the word alum was in Herodotus' 'The Persian Wars' (425 BC), Book II), but the word's appearance is only in Latinised translations made by Roman scholars in later centuries, and its reference is to a form of currency, not a description of the material or its uses. In 1781, de Morveau proposed the new-Latin term *alumine* (alumina in English) for the base in alum. In 1787 Lavoisier suggested that *alumine* was the oxide of a previously undiscovered metal. The word aluminum, later aluminium, was proposed by Davy in 1807, who confirmed that alumina has a metallic base.

Bauxite, the most common ore of aluminium, was discovered in 1821 by Berthier near the village of Les Baux, France. However, it was not until the end of the 19th century that bauxite was recognised as containing $\text{Al}(\text{OH})_3$ and $\text{AlO} \cdot \text{OH}$ and

various quantities of aluminium silicate, titanium dioxide and iron mineral impurities (Wefers and Misra 1987). It has since been determined that various crystallographic forms of the aluminium hydroxides including gibbsite, bayerite, boehmite, and diasporite may be present in the aluminium ores. It is from naturally occurring aluminium hydroxides, such as those found in bauxite, that alumina (Al_2O_3) is most commonly produced. This is primarily achieved using the Bayer process, developed in 1889 by Karl Bayer (Hind *et al.* 1999), which today remains the most economic thermal treatment for the synthesis of alumina.

Although aluminium is generally accepted to have been first isolated in 1825 by Hans Christian Oersted, Pliny may have unknowingly provided us with some curious insight into the history of alumina and aluminium with this excerpt from *Historia Naturalis* (77 AD, Book XXXV):

"One day a goldsmith in Rome was allowed to show the Emperor Tiberius a dinner plate of a new metal. The plate was very light, and almost as bright as silver. The goldsmith told the Emperor that he had made the metal from plain clay. He also assured the Emperor that only he, himself, and the gods knew how to produce this metal from clay. The Emperor became very interested, and as a financial expert he was also a little concerned. The Emperor felt immediately, however, that all his treasures of gold and silver would decline in value if people started to produce this bright metal from clay. Therefore, instead of giving the goldsmith the regard expected, he ordered him to be beheaded."

It can be conjectured that the metal is aluminium and the clay is an aluminium ore, such as bauxite, most likely from the now known deposits around the northern Mediterranean, once a part of ancient Rome's massive empire. Tiberius' (42 BC -- 37 AD) rashness appears to have deprived ancient Rome of a precious commodity with which to trade and the world of a long history of alumina and aluminium use. However, conclusive evidence of widespread Roman knowledge of alumina may yet be uncovered. It was not until the 18th and 19th centuries that the Western world only began to catch up to the Romans in most areas, including education, technology and administration. Moreover, new discoveries are being made about the Romans every

day. It has, for example, only recently been realised that Roman medical and surgical procedures, including eye, cosmetic and brain surgery, were on par with their modern counterparts, at least to the mid 20th century (Jackson 1991; Adkins and Adkins 1994; Shelton 1997). A future discovery of direct evidence of Roman knowledge of alumina and aluminium may not be surprising.

Today the word “alumina” is still vaguely used in literature to denote anything from the entire group of aluminous materials, including aluminium hydroxides. The definition of alumina by the Oxford English Dictionary (1989) illustrates some of the ambiguity in the use of the word: *“one of the earths, a white, insoluble, tasteless, amorphous substance; the only oxide (Al_2O_3) of the metal aluminium, the basis of alum, the chief constituent of all clays, and found crystallised as the sapphire.”* A quick browse through several dictionaries will show that most also refer to alumina as *“a mineral occurring in nature as corundum.”* The absence of universal standard nomenclature contributes to the confusion which has arisen in literature for the naming of aluminium compounds. Only one attempt has been made at implementing standardised nomenclature so far (Ginsberg *et al.* 1957). One of the outcomes of this attempt is that the prefix α is applied to hexagonal close packed and related structures while γ signifies cubic close packed and related structures.

Although there is loose and varied use of “alumina” as a naming tool, it definitively only applies to substances with the Al_2O_3 stoichiometric formula. Early research into aluminium compounds resulted in the discovery of aluminium ores, chiefly comprised of aluminium hydroxides. These aluminium hydroxides are sometimes, and incorrectly, referred to as hydrated aluminas. This misconception has resulted from the representative stoichiometric formulae; gibbsite, for example, is a trihydroxide compound ($Al(OH)_3$) which has been represented as $Al_2O_3 \cdot 3H_2O$ and named alpha aluminium hydrate by Alcoa (Wefers and Misra 1987).

The Transition Alumina's

It was eventually discovered that alumina itself also exists in a variety of ‘transition’ structures which are reproducible and stable at room temperature. The term ‘transition,’ as opposed to ‘metastable,’ applies as the phase transition between them is irreversible and occurs only with increasing temperature. The transition

aluminas occur within several pathways when dehydrating the aluminium hydroxides, such as gibbsite, to form *corundum* ($\alpha\text{-Al}_2\text{O}_3$), a name that lends itself from the mineral of composition Al_2O_3 identified in India by Greville in 1798 (van Horn *et al.* 2002). The α phase is the only thermodynamically stable oxide of aluminium and is the final product of the calcination process which follows the Bayer treatment. The nature of these phase transformations has now been studied for many years, and the pathways involved in the calcination include gibbsite \rightarrow boehmite ($\gamma\text{-AlOOH}$) \rightarrow γ -alumina ($\gamma\text{-Al}_2\text{O}_3$) \rightarrow δ -alumina ($\delta\text{-Al}_2\text{O}_3$) \rightarrow θ -alumina ($\theta\text{-Al}_2\text{O}_3$) \rightarrow α -alumina (Figure 1.1), with each transition phase exhibiting a distinct powder X-ray diffraction pattern. These phase transformations are of fundamental importance in designing ceramic processing procedures that use partially-calcined starting material.

Initial classification of the transition aluminas was by Ulrich (1925) who used the prefix γ for an undescribed alumina compound. This prefix has subsequently been used for all newly encountered and undescribed aluminas, all of which were found to form at low calcination temperatures during the thermal treatment of aluminium hydroxides. As new forms have been identified they have been assigned a unique Greek letter prefix. The γ prefix has since been restricted to the name of the structure obtained for the dehydration sequence of boehmite from 400 °C. Several other transitions have now been identified including the η , θ , κ , β , and χ aluminas. They are designated as oxides but it is not yet certain that they are anhydrous and several of the structures exhibit some amorphous content, hence they are commonly referred to as partially-calcined or partially dehydrated. A summary of the transformation transition aluminas and their occurrence in the calcination pathways is provided in Figure 1.1. Diagrams such as this serve only as a guide because they do not elucidate that the exact temperature of formation depends on parameters such as pressure and that overlap of phases can occur at certain temperatures.

The original purpose for the production of $\alpha\text{-Al}_2\text{O}_3$ was as a precursor in the production of aluminium metal which is the third most abundant element in the earth's crust, comprising 8.13%, and has almost limitless applications in transport, packaging, electrical, construction and medicine. In 2001, 48,488,000 metric tons of alumina was produced (Report 2001b). Of this figure 3,997,000 metric tons represents the amount of all phases of alumina produced for uses other than the

production of aluminium metal. The remaining alumina produced was used to synthesise 20,551,000 metric tons of aluminium (Report 2001a; Report 2001b).

Corundum itself has since found an enormous range of technological and industrial applications as a result of its hardness, abrasion resistance, mechanical strength, corrosion resistance, and good electrical insulation (Stumpf *et al.* 1950; Kingery *et al.* 1976). It is the most widely used form of alumina with structural, refractory, abrasive, optical, and electronic applications. Many of its applications are commonly known, such as its incorporation in composites (Green *et al.* 1989), while others are more obscure, such as its use in ballistic armour (Badmos and Ivey 2001).

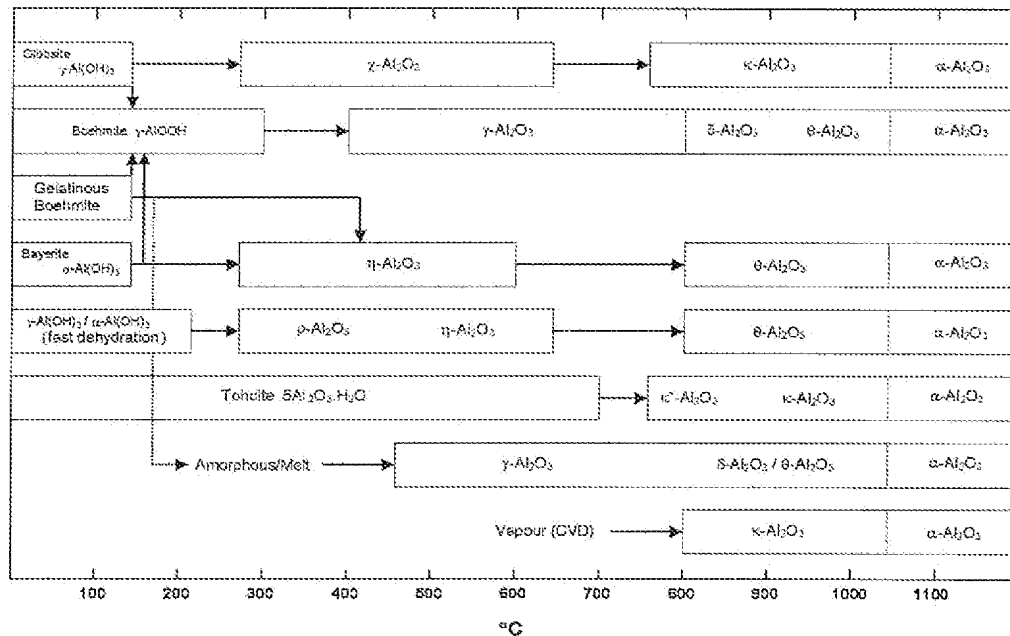


Figure 1.1. Commonly accepted transition sequences of the aluminas from hydroxides to corundum during thermal treatment (Wefers and Misra 1987; Levin

The industrial importance of transition aluminas is increasing as more becomes known about them. This group of materials have a variety of niche applications, many overlapping with those of α - Al_2O_3 , depending on the properties of the specific polymorph. κ -Alumina (κ - Al_2O_3), for example, finds use in wear-resistant coatings on cemented carbide cutting-tools (Lux *et al.* 1986; Vuorinen and Skogsmo 1990). δ -Alumina has been incorporated in bioactive bone cement

composites as a replacement for α - Al_2O_3 (Nishio *et al.* 2001). It was found to be superior for incorporation in bone cement as it allowed for greater osteoblastic differentiation than α - Al_2O_3 , allowing for *in-vivo* bone formation. θ -Alumina is used as a precursor for the production of ultra-high purity α - Al_2O_3 with reduced particle agglomeration (Wei *et al.* 1996; Kao and Wei 2000). All the transition aluminas have chemical functions including use as adsorbents, desiccants and binders. They are also widely used in heterogeneous catalysis, (Knözinger 1985) both as catalysts and support material for monolayer catalysts (Poncelet *et al.* 1991).

The transition aluminas are also of great importance in aluminium metal production. The α phase is not as soluble as the transition aluminas in the electrolytic solution (cryolite – Na_3AlF_6) from which aluminium metal is produced. Hence the processed alumina used for aluminium metal production contains a high amount of various transition phases (Homsí 1989; Hind *et al.* 1999). The high surface area, and corresponding adsorption properties, of some of the transition phases allows the alumina product to also be used as a HF (hydrogen fluoride) ‘scrubber’, during aluminium refinement in order to reduce HF pollution (Gillespie *et al.* 1999). Alumina has traditionally been formed by calcining aluminium trihydrate (gibbsite) in a rotary kiln at typically 1000 °C. More recently, fluidised bed furnaces have been used as they have more flexible calcination parameters, therefore exerting more influence on the amount of transition phases produced within the alumina product.

There still exists considerable controversy over the definitive structures of many of the alumina phases. In the case of δ - Al_2O_3 , there is speculation as to whether it exists at all. Studies by Zhou and Snyder (1991) and Gan (1996) have not reported the presence of δ - Al_2O_3 in the transformation sequence of γ - Al_2O_3 to θ - Al_2O_3 . Also, Pecharroman (1999) suggests that while δ - Al_2O_3 was detected using X-ray diffraction, it is actually a heterogeneous mixture of well crystallised γ - Al_2O_3 and θ - Al_2O_3 instead of a single δ -phase. Furthermore, many researchers who develop Al_2O_3 -based applications have not or are unable to ascertain the exact Al_2O_3 phase present. An example of this scenario is in the development of nanosized Al_2O_3 fibres. Two variants of Al_2O_3 nanofibres were developed by Tepper, Lerner and Ginley (2001) for improved catalysis, chemisorption of metals, use in nanocomposites, ceramic substrates, filters and membranes, and chemisorption and biomedical applications. These authors, however, have not identified a specific Al_2O_3

phase beyond the presence of amorphous Al_2O_3 . Without adequate knowledge of the structural form, research into the properties, dynamics and applications of these materials will always be less than optimal.

γ -Alumina

γ -Alumina, the subject of this thesis, is a material of immense industrial significance and is the subject of considerable research. It is used as a catalyst support for automotive (Satterfield 1980; Taylor 1993; Gates 1995) and industrial catalysts (Che and Bennett 1989; Xu *et al.* 1994), for example, the production of bulk and fine chemicals (Shi and Davis 1995), and as a catalyst in hydrocarbon conversion for petroleum refining (Tung and Mcininch 1964; Knözinger and Ratnasamy 1978). Supported catalysts are typically made by impregnating a porous material with an aqueous catalytic salt followed by calcination. Porosity is the property which makes $\gamma\text{-Al}_2\text{O}_3$ appealing as a catalyst support. Also, porosity (and therefore high surface area), combined with the removal of water and/or hydroxyl ligands at the surface, resulting in the exposure of Al^{3+} ions, are why $\gamma\text{-Al}_2\text{O}_3$ is also used directly as a catalyst.

Catalytic processes account for the majority of applications of $\gamma\text{-Al}_2\text{O}_3$. However, there are a growing number of other uses for $\gamma\text{-Al}_2\text{O}_3$. Like other transition aluminas, it is widely used as a polishing abrasive and in ceramic coatings, which provide corrosion, thermal and wear protection (McPherson 1980). NASA utilised it in $\gamma\text{-Al}_2\text{O}_3$ /epoxy composite struts to attach a cryogenically cooled solid-hydrogen telescope to its Wide-Field Infrared Explorer (WIRE) spacecraft because of its low thermal conductivity and relatively high mechanical strength (Rosanova 1998; Everett *et al.* 2000). Also, the high surface area of $\gamma\text{-Al}_2\text{O}_3$ makes it useful as platinum-coated combustion burners in recently investigated miniature power supplies (Drost *et al.* 1997; Koeneman *et al.* 1997). Furthermore, $\gamma\text{-Al}_2\text{O}_3$ has also been shown to be thermodynamically stable relative to $\alpha\text{-Al}_2\text{O}_3$ when a critical surface area is achieved (McHale *et al.* 1997). The outcomes of this research can open up endless possibilities for applications of $\gamma\text{-Al}_2\text{O}_3$.

The Uncertainty Surrounding γ -Alumina

Despite the industrial significance of γ -Al₂O₃, controversy still exists over its definitive structure. Not even the mechanisms by which γ -Al₂O₃ behaves as a catalyst (or support) are clearly understood (Sohlberg *et al.* 1999; Xia *et al.* 1999). Over 67 years have passed since the first description of its structure, which was as a cubic spinel-type (MgAl₂O₄) structure (Verway 1935a), and over 52 years since it was identified as a direct product of the calcination of boehmite (Stumpf *et al.* 1950). Yet there are still many questions regarding its formation, structure, and even stoichiometry. It was initially determined to occur at a calcination temperature of > 525 °C, though now it is thought to occur between 400 and 950 °C (Stumpf *et al.* 1950; Saalfeld 1958; Lippens and de Boer 1964). These early studies have tended to shed light on the configuration of the oxygen sublattice, however the major uncertainty arises in the positions of the aluminium ions within the unit cell. Analysis of neutron, X-ray, and electron diffraction data, has led to conclusions that the vacancies are situated entirely on octahedral (Sinha and Sinha 1957; Jagodzinski and Saalfeld 1958; Li *et al.* 1990; Wang *et al.* 1998; Kryukova *et al.* 2000) or tetrahedral (Saalfeld 1958; Saalfeld and Mehrotra 1965; Jayaram and Levi 1989) sites, or distributed over both spinel site positions (Wilson 1979; Wang *et al.* 1999). The occupation of a highly distorted Wyckoff 32*e* site has also been reported (Zhou and Snyder 1991; Gan 1996), which coincides with reports of 'pentahedrally' coordinated Al by several NMR studies (Dupree *et al.* 1986; Chen *et al.* 1992; Pecharroman *et al.* 1999; Wang *et al.* 1999). Furthermore, there is the issue of hydrogen and/or water content in the lattice, which remains unsolved.

Three space groups have been attributed to the γ -Al₂O₃ structure; $Fm\bar{3}m$, $Fd\bar{3}m$ and $I4_1/amd$. It is traditionally thought to be a cubic spinel structure, but tetragonally-distorted structures have been reported (Stumpf *et al.* 1950; Lippens and de Boer 1964). Wilson (1979) and Wilson and McConnell (1980) also observed a tetragonally-distorted spinel structure for γ -Al₂O₃, but found that distortion of the spinel lattice decreases with increasing time or temperature of heat treatment. They found this decrease of tetragonal γ -Al₂O₃ coincide with the formation of cubic γ -Al₂O₃. Zhou and Snyder (1991) found the structure to be a cubic spinel, reporting no tetragonal distortion. Later, Gan (1996), suggested tetragonal and cubic γ -Al₂O₃ to

be simultaneously present at all temperatures with the tetragonal form dominating at lower temperatures. The amount of cubic $\gamma\text{-Al}_2\text{O}_3$ was suggested to increase with increasing temperature, at the expense of tetragonal $\gamma\text{-Al}_2\text{O}_3$.

Through extensive reading one can see that many subtle, confusing and contradictory variations of the structure of $\gamma\text{-Al}_2\text{O}_3$ (and $\delta\text{-Al}_2\text{O}_3$) have been reported. There has even been one study which has reported a supercell lattice parameter of 15.790 Å as opposed to the traditionally known ~ 7.9 Å (Kordes 1935). One can see that there is a myriad of preparation routes. Further confusion has been added by the terminology used to describe these structures. For example, Rooksby and Rooymans (1961) labelled the tetragonally distorted $\gamma\text{-Al}_2\text{O}_3$ structure described by Saalfeld (1958) as $\delta\text{-Al}_2\text{O}_3$ which was later confirmed, by Lippens and de Boer (1964) to be $\gamma\text{-Al}_2\text{O}_3$. It appears that the exclusive use of traditional experimental techniques will fall short of providing a decisive answer. Understanding the structure of $\gamma\text{-Al}_2\text{O}_3$ has far reaching implications. Some researchers, in their study of the structure and phase transformation to $\delta\text{-Al}_2\text{O}_3$ and, subsequently, $\theta\text{-Al}_2\text{O}_3$, have assumed a structure for $\gamma\text{-Al}_2\text{O}_3$ (Levin *et al.* 1997; Levin and Brandon 1998b; Levin *et al.* 1998). The advantage in knowing the structure of $\gamma\text{-Al}_2\text{O}_3$ for such a study is obvious. It is an imperative step towards understanding mechanisms of phase transformation. It will assist in the subsequent understanding of the surface structure of $\gamma\text{-Al}_2\text{O}_3$. Furthermore, it will ultimately assist in understanding the mechanism by which $\gamma\text{-Al}_2\text{O}_3$ behaves as a catalyst, and will allow for synthesis techniques to be refined and lead to further development of applications.

Problems Associated with Solving $\gamma\text{-Alumina}$

The predominant factor hindering attempts to solve the $\gamma\text{-Al}_2\text{O}_3$ structure is that it is poorly ordered. This makes it difficult to obtain single crystals of suitable size (coherently scattering domains do not usually exceeding 300 nm), and hence, unsuitable for single-crystal diffraction studies. Furthermore, powder diffraction patterns exhibit high backgrounds and diffuse peaks. The structural disorder makes it difficult to obtain electron diffraction patterns as kikuchi bands, which are used to

identify zone axes, are generally not observed. These complications make it difficult to determine the structure unambiguously.

The traditionally used powder X-ray diffraction and electron microscopy are at a disadvantage when examining the complicated structures of the Al_2O_3 polymorphs. These structures have similar d-spacings and the transformations appear to occur continuously, with several phases coexisting in some instances. Furthermore, factors such as the degree of crystallinity, the presence of impurities, particle size and pressure can alter when a transformation occurs and affect what variant of the structure will be found. Powder X-ray diffraction, where the analysis is 'averaged' over thousands of crystals cannot adequately overcome these problems, while the use of electron microscopic techniques may sometimes be too arduous to cover the scope of all possibilities. A possible solution is offered by the use of computational molecular modelling techniques, in conjunction with suitable experimental analysis.

In recent years rapid advancement has occurred in the field of computational materials science. Huge advances in computing power during this period have made it possible to apply the laws of quantum mechanics to the study of macroscopic properties of real materials at the atomic level. Predicting the properties of materials by theoretical means can achieve high accuracy and complements the traditional experimental approaches. In many cases, time and money can be saved by conducting theoretical simulations on a material before conducting experimental tests.

Ab initio quantum mechanical calculations of a single configuration of complex structures like $\gamma\text{-Al}_2\text{O}_3$ can take many days or weeks, whereas the empirical modelling methods, which are based on classical physics, typically only involve a few minutes of computation time. This allows for many more possible structural candidates to be examined, in order to thoroughly sample configuration space, for disordered materials. Although modelling techniques based on interatomic potentials cannot yield accurate data with regards to electronic properties of materials, they can produce reasonably accurate structural data in a fraction of the time taken by quantum mechanical calculations. This means that interatomic potentials can be used to reduce the number of likely candidates before utilising a first principles approach. A key advantage to theoretical investigations is the ability to directly examine many

possible structures of the material, whereas traditional experimental techniques usually correspond to one general model being conceptualised. Hence, this research will involve the combined use of interatomic potentials and first principles calculations, by means of density functional theory (DFT), to investigate possible structures of $\gamma\text{-Al}_2\text{O}_3$ and yield highly accurate results.

Whereas structure determination problems are traditionally approached by obtaining a diffraction pattern and working backwards to determine the unit cell, with interatomic potentials and DFT the process of structure determination begins with construction of the unit cell which is then optimised. The final possible structures determined are then compared with experimental data to obtain consensus. The theoretical modelling will provide a representative structure for $\gamma\text{-Al}_2\text{O}_3$ with precise cation coordinates. To date no experimental study has provided precise cation coordinates for $\gamma\text{-Al}_2\text{O}_3$, a limiting factor brought about by the nature of the material.

1.1 Objectives

The aim of the work contained within this thesis is to advance knowledge of and make new insights into the structure of $\gamma\text{-Al}_2\text{O}_3$. Research will be primarily geared towards elucidating the definitive structure and settling the ambiguity surrounding the $\gamma\text{-Al}_2\text{O}_3$ system. The primary technique to be used is computer simulations based on both interatomic potentials and first principle calculations. This will be combined with the following supporting experimental techniques:

- Neutron diffraction
- X-ray diffraction
- Transmission electron microscopy and electron diffraction
- Nuclear magnetic resonance spectroscopy
- Differential scanning calorimetry and thermogravimetric analysis
- Infra-red spectroscopy
- Inelastic neutron Scattering
- Prompt-gamma activation analysis
- Small angle X-ray scattering
- BET and pycnometry
- Loss on ignition

- The computational work will involve the development of a methodology which will allow all structure possibilities to be examined and do so in reduced time. This is contrast to previous computational studies which have been time consuming and, because of this, have not been able to examine all possible structures.
- Focus will be directed towards accurately determining the unit cell and assessing the possibility of a dual-phase structure.
- Attention will be paid to ascertaining the distribution of vacancies and the precise cation coordinates.
- Once a satisfactory structural model is established annealing time and temperature effects on the system will be examined.
- Research will also involve understanding the evolution of the structure as the transition sequence progresses. The nature of hydrogen and its role in the structure of $\gamma\text{-Al}_2\text{O}_3$ will also be investigated.
- An understanding of the possible synthesis techniques and kinetic effects will be developed with the view of employing a common approach to produce a systematic set of samples within the temperature range of the occurrence of $\gamma\text{-Al}_2\text{O}_3$ for study using experimental techniques.

In addition to the extension of the current understanding the results will offer a platform for further study of the system and other similar and related systems, such as η and $\delta\text{-Al}_2\text{O}_3$.

Faculty of Science
Department of Applied Physics
and
Department of Applied Chemistry

**Determination of the Structure of γ -Alumina using
Empirical and First Principles Calculations combined with
Supporting Experiments**

Gianluca Paglia

This thesis is presented for the Degree of
Doctor of Philosophy
of
Curtin University of Technology

February 2004

Declaration

This thesis contains no material which has been accepted for the award of any other degree or diploma in any university.

To the best of my knowledge and belief this thesis contains no material previously published by any other person except where due acknowledgement has been made.

Signature:

A handwritten signature in black ink, consisting of a large, stylized 'D' followed by a horizontal line and a small flourish.

Date:

February 2nd 2004

Acknowledgments

One can never know how difficult putting together a PhD thesis can be until one actually goes through the process. I myself did not appreciate this until I tried it myself. And now a days there is enormous pressure to complete the work within three odd years. I am enormously proud of the work which constitutes this thesis. It can be justifiably split up into two projects. However, such a task could not be achieved without the valuable aid of many people, without which I would not have been able to do this at all.

Before mentioning the people directly I would like to thank several institutions for providing financial support. Firstly, the Australian government for awarding me with an Australian Post-Graduate Award with Stipend (APAWS). The Australian Institute of Nuclear Science and Engineering (AINSE) for awarding me with a Post-Graduate Research Award (PGRA) which includes a scholarship and a grant to travel to the Australian Nuclear Science and Technology Organisation (ANSTO), Lucas Heights, Sydney to perform key experiments for the project. The staff at AISNE were very friendly and always accommodating to my needs. I thank them kindly. Thanks also goes to the Western Australian Interactive Virtual Environments Centre (IVEC) and the Australian Partnership for Advanced Computing (APAC) for provision of allocation time on their computational facilities. IVEC also kindly awarded me with a Western Australian IVEC Doctoral Scholarship (WAIDS).

The most important people to thank are my two supervisors, Associate Professors Craig Buckley (Materials Research Group) and Andrew Rohl (Nanochemistry Research Institute). The project was originally Craig's idea. He, in partnership with Andrew won an ARC Small Grant to purchase some of the software and equipment necessary to carry out the work. Craig taught me much about concepts in physics that I was yet to grasp properly. He also helped me enormously in getting started with computer programming. In spite of his own enormously busy schedule, time was always made for me to seek advice, without having to make an appointment in advance. I sought advice frequently. He also provided advice that extended beyond issues pertaining to the project work, such as career and personal concerns. Importantly, both he and Andrew allowed me to take control of the project

and do things how I saw best, which facilitated a casual, yet productive, atmosphere. I consider him to be an excellent friend and mentor.

Andrew's assistance in the project was invaluable. Without his assistance and the resources already under his control, the degree of modelling that was performed would not have been achieved. It was through Andrew that I learnt most about the concepts of molecular modelling. He was also the person I came to rely on most with developing my programming skills. As with Craig, I frequently sought his assistance because the learning curve for both the modelling and programming was enormous. Like Craig, he has become an excellent friend and mentor.

The computational work was carried out using two simulation codes, GULP and SIESTA, which were acquired through Professor Julian Gale, who has recently moved to Curtin University from Imperial College, London. He is the author of the former program and a co-developer of the latter. Julian's assistance has been invaluable. He provided a lot of assistance with the use of both codes and helped me to understand a lot of the concepts behind the programs.

Professor Brian O'Connor was the main person who motivated me to undertake my Ph.D. The project was jointly his conception, with Craig. It was Brian's idea to make γ -alumina as the subject of this modelling-based project. Brian has produced a wealth of research on transition aluminas so his advice was very useful and greatly appreciated. Although we did not always agree, a compromise was always achievable. I have enormous respect for his scientific achievements.

Most of the assistance I received for my experimental work was provided by Dr Robert Hart and Karsten Winter from the Materials Research Group and Dr's Brett Hunter and Andrew Studer from the Bragg Institute at ANSTO. Robert was with me every minute while performing electron microscopy. He did most of the difficult fine-tuning required to obtain high quality images and diffraction patterns, saving me an enormous amount of time. He taught me how to analyse the patterns and about the associated crystallography. He also helped me improve my scientific writing and reduce the amount of words used. In this area, I was certainly in need of improvement. The electron microscopy work could not have been done without the contribution made by Professor Arie van Riessen. Arie was an associate supervisor to the project. While the nature of the project was such that he was not able to provide much direct assistance he is the person behind the obtainment of the state of the art

electron microscopy equipment for the physics department. He is also responsible for the appointment of Robert Hart to the run the equipment. He is the first scientist I had respect for and always made himself available for discussion when I sought advice on matters.

Karsten Winter was an integral part of this project. Although he is a fellow PhD student he has over 15 years experience in crystallography. He helped me understand vital crystallographic concepts which I had never before been properly exposed to nor could I have hoped to learn it without many years of hard reading. This facilitated rapid output of written work on my part. Without this help, the project would easily have take up to a year longer. He is an excellent mentor.

Brett Hunter, my AINSE supervisor, and Andrew Studer assisted me in performing the neutron diffraction experiments at ANSTO. Their assistance was therefore imperative. Andrew taught me how to use the processing software developed at ANSTO to convert the data to the correct format and perform all the necessary precursory analysis before performing Rietveld analysis. He also did much of the legwork to keep the experiments running smoothly. Brett is the author of Rietica and taught me most of what I know about Rietveld Analysis. Dr Margaret Elcombe, from the Bragg Institute, was also a key factor in helping me to understand Rietveld analysis. In all, I spent about seven to eight weeks conducting experiments at ANSTO. All of the staff made me feel very welcome. Professor Robert Robinson gave me great advice on my future. Spending time working at another institution was an excellent experience.

Other people from ANSTO, from the Materials Division, also made extremely important contributions. John Hanna performed the high-resolution NMR experiments and David Cassidy performed the BET and pycnometry.

Dr Lindsey Byrne from the NMR facility at the University of Western Australia collected my initial NMR data and facilitated my analysis of the all the data by providing me with access to the appropriate software. Nigel Kirby and Geoff Carter from the Materials Research Group also helped with BET work.

Clinton Maitland and Dr Joan Connolly from the Materials Research Group and Dr Terry Udovic of the National Institute of Standards and Technology (NIST), USA also deserve a big thank you. Clinton and Joan performed small angle X-ray scattering on my samples and Clinton did the modelling analysis. Terry performed the neutron vibrational spectroscopy and prompt-gamma activation analysis. They

made life very easy for me as they supplied the results and all I had to do was interpret the significance.

Special thanks goes to Professor Li Deyu of the Materials Research Group. Li helped me to get started with the basics of Rietveld analysis. He provided me with insight regarding what had been previously done on γ -alumina within the department and supplied me with the conference paper he, Brian and co. authored in 1990.

There have been several other people who have provided valuable assistance. Dr Franca Jones, Nanochemistry Research Institute, helped me to conduct the infrared analysis of my samples. Dr Andrew Fogg, formerly of the Nanochemistry Research Institute, allowed me to use his Bayer labs to synthesise my gibbsite and boehmite starting materials. Dr Joanne Loh, formerly a Ph.D. student with the Nanochemistry Research Institute provided useful comments and taught me how to synthesise hydrogenated and deuterated gibbsite. John Cornell of ALCOA World Alumina supplied me with commercial boehmite from the Alumina and Ceramics Laboratory, Malakoff Industries, Arkansas, USA. Professor Andrew Johnson of the Centre for Microscopy and Microanalysis at the University of Western Australia provided valuable advice and helped me obtain my first electron diffraction pattern of γ -alumina. Dr Sean Fleming, helped me with IT issues pertaining to the molecular modelling. I must also thank Professor Javier Junquera for kindly generating the optimized basis sets used in this work.

I was also given tremendous help from two good friends of mine, Damien Carter, fellow Ph.D. student from the Nanochemistry Research Institute, and Dr Justin Hoffman, formerly a Ph.D. student of the Department of Applied Physics. These gentlemen helped me with many IT issues.

Every one of these people has taught me something. They have all made some form of impact on my life. I thank them and all my other colleagues for their friendship and encouragement. The road certainly would have been much harder if they weren't there. I am extremely grateful.

I must also thank my fiancé, Vanessa Di Falco, for all her support. She has been very understanding with all the long hours that I have had to put in and has kept my belly fully on many occasions. She has taken my aloofness and many nights spent indoors with a notebook computer on my lap surprisingly well. Her love has been unconditional. I dedicate this work to her and our future together.

29/11/2003

Abstract

Aluminas have had some form of chemical and industrial use throughout history. For little over a century corundum (α - Al_2O_3) has been the most widely used and known of the aluminas. The emerging metastable aluminas, including the γ , δ , η , θ , κ , β , and χ polymorphs, have been growing in importance. In particular, γ - Al_2O_3 has received wide attention, with established use as a catalyst and catalyst support, and growing application in wear abrasives, structural composites, and as part of burner systems in miniature power supplies. It is also growing in importance as part of the feedstock for aluminium production in order to affect both the adsorption of hydrogen fluoride and the feedstock solubility in the electrolytic solution. However, much ambiguity surrounds the precise structure of γ - Al_2O_3 . Without proper knowledge of the structure, understanding the properties, dynamics and applications will always be less than optimal.

The aim of this research was to contribute towards settling this ambiguity. This work was achieved through extensive computer simulations of the structure, based on interatomic potentials with refinements of promising structures using density functional theory (DFT), and a wide range of supporting experiments. In addition to providing a more realistic representation of the structure, this research has also served to advance knowledge of the evolution of the structure with changing temperature and make new insights regarding the location of hydrogen in γ - Al_2O_3 .

Both the molecular modelling and Rietveld refinements of neutron diffraction data showed that the traditional cubic spinel-based structure models, based on $Fd\bar{3}m$ space group symmetry, do not accurately describe the defect structure of γ - Al_2O_3 . A more accurate description of the structure was provided using supercells of the cubic and tetragonal unit cells with a significant number of cations on c symmetry positions. These c symmetry based structures exhibited diffraction patterns that were characteristic of γ - Al_2O_3 .

The first three chapters of this Thesis provide a review of the literature. **Chapter One** provides a general introduction, describing the uses and importance of the aluminas and the problems associated with determining the structure of γ - Al_2O_3 . **Chapter Two** details the research that has been conducted on the structure of

γ -Al₂O₃ historically. **Chapter Three** describes the major principles behind the computational methods employed in this research.

In **Chapter Four**, the specific experimental and computational techniques used to investigate the structure of γ -Al₂O₃ are described. All preparation conditions and parameters used are provided.

Chapter Five describes the methodology employed in computational and experimental research. The examination of the ~ 1.47 billion spinel-based structural possibilities of γ -Al₂O₃, described using supercells, and the selection of $\sim 122,000$ candidates for computer simulation, is detailed. This chapter also contains a case study of the structure of κ -Al₂O₃, used to investigate the applicability of applying interatomic potentials to solving complex structures, where many possibilities are involved, and to develop a systematic procedure of computational investigation that could be applied to γ -Al₂O₃.

Chapters Six to Nine present and discuss the results from the experimental studies. Preliminary heating trials, performed to determine the appropriate preparation conditions for obtaining a highly crystalline boehmite precursor and an appropriate calcination procedure for the systematic study of γ -Al₂O₃, were presented in **Chapter Six**.

Chapter Seven details the investigation of the structure from a single-temperature case. Several known structural models were investigated, including the possibility of a dual-phase model and the inclusion of hydrogen in the structure. It was demonstrated that an accurate structural model cannot be achieved for γ -Al₂O₃ if the cations are restricted to spinel positions. It was also found that electron diffraction patterns, typical for γ -Al₂O₃, could be indexed according to the $I4_1/amd$ space group, which is a maximal subgroup of $Fd\bar{3}m$. Two models were presented which describe the structure more accurately; Cubic-16c, which describes cubic γ -Al₂O₃ and Tetragonal-8c, which describes tetragonal γ -Al₂O₃. The latter model was found to be a better description for the γ -Al₂O₃ samples studied.

Chapter Eight describes the evolution of the structure with changing calcination temperature. Tetragonal γ -Al₂O₃ was found to be present between 450 and 750 °C. The structure showed a reduction in the tetragonal distortion with increasing temperature but at no stage was cubic γ -Al₂O₃ obtained. Examination of the progress of cation migration indicates the reduction in the tetragonal nature is due

to ordering within inter-skeletal oxygen layers of the unit cell, left over from the breakdown of the hydroxide layers of boehmite when the transformation to $\gamma\text{-Al}_2\text{O}_3$ occurred. Above 750 °C, $\delta\text{-Al}_2\text{O}_3$ was not observed, but a new phase was identified and designated $\gamma'\text{-Al}_2\text{O}_3$. The structure of this phase was determined to be a triple cell of $\gamma\text{-Al}_2\text{O}_3$ and is herein described using the $P\bar{4}m2$ space group.

Chapter Nine investigates the presence of hydrogen in the structure of $\gamma\text{-Al}_2\text{O}_3$. It was concluded that $\gamma\text{-Al}_2\text{O}_3$ derived from highly crystalline boehmite has a relatively well ordered bulk crystalline structure which contains no interstitial hydrogen and that hydrogen-containing species are located at the surface and within amorphous regions, which are located in the vicinity of pores. Expectedly, the specific surface area was found to decrease with increasing calcination temperature. This trend occurred concurrently with an increase in the mean pore and crystallite size and a reduction in the amount of hydrogen-containing species within the structure. It was also demonstrated that $\gamma\text{-Al}_2\text{O}_3$ derived from highly crystalline boehmite has a significantly higher surface area than expected, attributed to the presence of nano-pores and closed porosity.

The results from the computational study are presented and discussed in **Chapter Ten**. Optimisation of the spinel-based structural models showed that structures with some non-spinel site occupancy were more energetically favourable. However, none of the structural models exhibited a configuration close to those determined from the experimental studies. Nor did any of the theoretical structures yield a diffraction pattern that was characteristic of $\gamma\text{-Al}_2\text{O}_3$. This discrepancy between the simulated and real structures means that the spinel-based starting structure models are not close enough to the true structure of $\gamma\text{-Al}_2\text{O}_3$ to facilitate the derivation of its representative configuration. Large numbers of structures demonstrate migration of cations to c symmetry positions, providing strong evidence that c symmetry positions are inherent in the structure. This supports the Cubic-16c and Tetragonal-8c structure models presented in **Chapter Seven** and suggests that these models are universal for crystalline $\gamma\text{-Al}_2\text{O}_3$. Optimisation of c symmetry based structures, with starting configurations based on the experimental findings, resulted in simulated diffraction patterns that were characteristic of $\gamma\text{-Al}_2\text{O}_3$.

LIST OF ABBREVIATIONS

γ -Al ₂ O ₃	Gamma alumina
γ' -Al ₂ O ₃	Gamma-prime alumina
α -Al ₂ O ₃	Alpha alumina
δ -Al ₂ O ₃	Delta alumina
θ -Al ₂ O ₃	Theta alumina
κ -Al ₂ O ₃	Kappa alumina
η -Al ₂ O ₃	Eta alumina
χ -Al ₂ O ₃	Chi alumina
AINSE	Australian Institute of Nuclear Science and Engineering
ANSTO	Australian Nuclear Science and Technology Organisation
APW	Augmented plane waves
BFGS	Broyden-Fletcher-Goldfarb-Shanno minimisation algorithm
CBED	Convergent beam electron diffraction
Cheby I	Non-shifted type 1 Chebyshev function
CSD	Coherently scattering domains
DRIFT	Diffuse Reflectance Infrared Fourier Transform
DTA	Differential thermal analysis
DZ	Double-zeta
DZP	Double-zeta plus polarisation
EDS	Energy dispersive spectrometry
FANS	Filter Analyser Neutron Spectrometer
FLAPW	Full-potential linear augmented plane waves
FWHM	Full-width-at-half-maximum
GEA	Gradient expansion approximation
GGA	Generalised gradient approximation
Gnorm	Normal to the energy gradient in GULP.
GTO	Gaussian-type-orbital
GULP	General utility lattice program
HF	Hartree-Fock
HRPD	High-resolution powder diffractometer
ICDD	International Centre for Diffraction Data

INS	Inelastic neutron scattering
IR	Infrared
ISIS	Name of the Spallation Neutron Source, UK.
LAPW	Linear augmented plane waves
LCAO	Linear combinations of atomic orbitals
LDA	Local density approximation
LSD	Local spin density approximation
MAS-NMR	Magic angle spinning nuclear magnetic resonance
MRPD	Medium-resolution powder diffractometer
NCNR	NIST Center for Neutron Research
ND	Neutron diffraction
NIST	National Institute of Standards and Technology, USA
NMR	Nuclear magnetic resonance
NVS	Neutron vibrational spectroscopy = INS
OLCAO	Orthogonalized linear combinations of atomic orbitals
PDF	Powder diffraction file
PGAA	Prompt gamma activation analysis
PW	Plane waves
RFO	Rational function optimisation
SAD/SAED	Selected area electron diffraction
SEM	Scanning electron microscopy
SIESTA	Spanish initiative for electronic simulations of thousands of atoms
STO	Slater-type-orbital
TED	Transition electron diffraction
TEM	Transición electron microscopy
TGA	Thermogravimetric analysis
XRD	X-ray diffraction

Contents

Acknowledgements	i
Abstract	v
List of Abbreviations	viii
Contents	x
List of Figures	xiv
List of Tables	xix
1.0 Introduction	1
<i>The Transition Alumina's</i>	3
<i>γ-Alumina</i>	7
<i>The Uncertainty Surrounding γ-Alumina</i>	8
<i>Problems Associated with Solving γ-Alumina</i>	9
1.1 Objectives	11
2.0 The Structure of γ-Alumina Explored: Historical Review	13
2.1 Preparation and Reaction Kinetics	13
2.1.1 Amorphous Precursors	19
2.2 Characterisation of the Crystallographic Structure	21
2.2.1 Structural Characteristics from Diffraction Patterns	23
2.2.2 Discrepancies in Cation Occupation	25
<i>Departure from Spinel Position Exclusivity</i>	26
2.2.3 Tetragonal Deformation in Boehmite Derived γ -Alumina	27
2.2.4 The Uncertain Role of Hydrogen	29
<i>Structural Aspects</i>	29
<i>Surface Structure</i>	32
2.2.5 Computational Investigations into γ -Alumina	35
3.0 Computational Techniques used <i>Abhinc</i>: Principles	39
3.1 Development of Atomic Theory	39
3.2 Computer Simulation of Atomic Structures	41
3.3 Empirical Force Field Molecular Mechanics	42
3.3.1 Interatomic Potentials	44
<i>Polarization</i>	45
3.3.2 Electrostatic Interactions	46
3.3.3 Energy Minimization	47

<i>Derivative Methods</i>	48
3.4 Density Functional Theory	51
3.4.1 Basic Quantum Mechanical Concepts	51
3.4.2 Components of the Total Energy in DFT	53
3.4.3 Hohenberg and Kohn Theorem	55
3.4.4 Self Consistent Kohn Sham Equations	56
3.4.5 Approximating Exchange and Correlation	59
<i>Generalised Gradient Approximation</i>	62
3.4.6 Basis Sets	63
<i>Plane Waves</i>	64
<i>Atomic Orbitals</i>	65
3.4.7 Pseudopotential Approximation	66
4.0 Deterministic Methods	69
4.1 Experimental	69
4.1.1 Materials and Sample Preparation	69
4.1.2 Particle Size Analysis	70
4.1.3 Thermal Analysis	70
4.1.4 X-ray Diffraction	71
4.1.5 Neutron Diffraction	71
4.1.6 Rietveld Analysis of Neutron Diffraction Data	72
4.1.7 Transmission Electron Microscopy and Electron Diffraction	75
4.1.8 Nuclear Magnetic Resonance	76
4.1.9 Small Angle X-ray Scattering	76
4.1.10 Method of SAXS Analysis	77
4.1.11 Multipoint BET Adsorption Isotherm and Density Measurements	79
4.1.12 Loss on Ignition	79
4.1.13 Prompt-Gamma Activation Analysis	80
4.1.14 Inelastic Neutron Scattering	80
4.1.15 Infrared Analysis	81
4.2 Computational	81
4.2.1 Interatomic Potential Calculations	81
4.2.3 First Principles Calculations	83
5.0 Methodology	85
Preamble	85
5.1 Experimental Methodology	88

5.1.1 Consideration of Hydrogen and Surface	89
5.2 Computational Methodology	90
5.2.1 Summary of Structure	90
5.2.2 Generation of Structural Candidates	92
<i>Selection Criteria</i>	94
<i>Nomenclature</i>	99
5.3 Case Study: Testing the Computational Approach with κ -Alumina	100
5.3.1 Why κ -Alumina?	100
5.3.2 Methodology	101
5.3.3 Structure Notation and Candidates	102
5.3.4. Results and Discussion: Interatomic Potentials	105
5.3.5. Implementation of Quantum Mechanical Calculations	115
5.3.6. Outcomes from Case Study	118
6.0 Preliminary Experimental Findings: Heating Trials	120
6.1 Procurement of Appropriate Boehmite Precursor	120
6.2 Establishing Suitable Calcination Procedures for Systematic Study of γ -Alumina	123
6.2.1 Thermal Analysis	123
6.2.2 Heating Trials for the Effect of Milling and Calcination Time	125
6.2.3 Kinetic Study of Neutron Diffraction Data Calcined <i>In Situ</i>	127
6.2.4 Outcomes Pertinent to this Study	129
7.0 Experimental Findings: Establishing a Representative Structural Model	130
Preamble	130
7.1 Initial Rietveld Refinement Trials	131
7.1.1 Starting Structure Models for Rietveld Analysis	131
7.1.2 Results from Initial Rietveld Analysis Trials	133
7.1.3 Conclusions from Preliminary Analysis	139
7.2 Development of a New Structural Model	140
7.2.1 Space Group Identification from TEM	144
7.2.2 Proposed Tetragonal Model	147
7.2.3 Consideration of Hydrogen	149
7.2.4 Outcomes from Study of Single Temperature Case	153
8.0 Experimental Findings: Structural Evolution with Temperature	156
Preamble	156
8.1 Morphology of Samples	157

8.2 Structural Variation with Temperature and the Identification of a New Phase, γ' -Alumina	162
8.3 Structural Details of γ -Alumina	168
8.4 Determination of the Structure of γ' -Alumina	172
8.5 Outcomes	178
9.0 Experimental Findings: Consideration of Hydrogen and Surface Effects	180
Preamble	180
9.1 Surface Area and Microstructure Trends	181
9.2 Measuring the Quantity of Hydrogen in the Structure	187
9.3 Neutron Vibrational Spectroscopy	190
9.4 Infrared Analysis	192
9.5 Outcomes	196
10.0 Computational Findings	198
Preamble	198
10.1 Spinel-Based Structure Candidates	199
10.1.1 Structure Analysis	201
10.2 More Appropriate Starting Models (<i>c</i> Symmetry Based)	209
10.2.1 Oxygen Sublattice Distortion During Optimisation	211
10.3 Results from Optimisation of <i>c</i> Symmetry Based Structures	212
10.3.1 Higher Accuracy Structure Examples	221
10.4 Outcomes	224
11.0 Conclusions	226
11.1 Recommendations	231
References	233
Appendix I – Particles Size Analysis Data	256
Appendix II – Rietveld Analysis Data for γ -Alumina	261
Appendix III – Rietveld Analysis Data for γ' -Alumina	275
Appendix IV – Supercell Coordinates	289
Appendix V – Selection Criteria	295
Appendix VI – Fortran Codes for Structure Generation	305
Appendix VII – Python Codes for Structure Analysis	317
Appendix VIII – Analysis Output for Optimised Structures	329
Appendix IX – Optimised Structural Coordinates	332
Appendix X – Publication List	340

List of Figures

Figure 1.1.	Commonly accepted transition sequences of the aluminas from hydroxides to corundum during thermal treatment.	5
Figure 2.1.	DTA curves of gibbsite for different particle sizes.	15
Figure 2.2.	Possible reaction pathways from alumina hydrates to the formation of γ -Al ₂ O ₃ .	18
Figure 2.3.	Most common electron diffraction pattern observed for γ -Al ₂ O ₃ , [0 kl] zone axis, depicting the position of reflections and each reflection type.	24
Figure 2.4.	Typical XRD pattern for γ -Al ₂ O ₃ , indexed according to the $Fd\bar{3}m$ space group.	25
Figure 3.1.	Overview of computational techniques available for solving the Kohn-Sham Equations; $V(r)$ represents $V_{ion}(r)$ and $V_H(r)$.	58
Figure 3.2.	Schematic illustration of the self-consistent iterative procedure used to solve electronic structure calculations.	59
Figure 3.3.	Pictorial representation of the local density approximation.	61
Figure 3.4.	Illustration of the pseudo-wavefunction (Ψ_{pseudo}) and potential (V_{pseudo}) and how they compare to the all-electron wavefunction (Ψ_{AE}) and electronic potential ($V_{ext} = Z/r$).	67
Figure 5.1.	Flowchart depicting the general methodology adopted in this research.	86
Figure 5.2.	Illustration of how each starting structural possibility is generated.	92
Figure 5.3.	Illustration of the selection criteria.	96
Figure 5.4.	Flow chart illustrating how application of the selection criteria reduce the number of structure candidates.	97
Figure 5.5.	Representative illustration of the energy distribution of the groups of structures with different mean number of nearest neighbours.	97
Figure 5.6.	Illustration of the stacking sequence of the oxygen sublattice and an idealised example of unit cell.	102
Figure 5.7.	Illustration of aluminium pair positions (labelled circles) between the A and B stacking layers of oxygen.	103
Figure 5.8.	Starting and minimised energies using the potentials of Bush <i>et al.</i> (1994).	106
Figure 5.9.	Minimised energies achieved for each of the potentials incorporated into the Buckingham Model.	107 108

Figure 5.10.	Lowest energy structure from fixed cell parameter minimisations; MO coordination; Atomic configuration: $Ac_{\alpha}c_{\beta}Bb_{\beta}c_{\gamma}Ab_{\alpha}byCb_{\beta}c_{\gamma}$.	109
Figure 5.11.	(a): Lowest energy structure determined using the potential parameters of Catlow <i>et al.</i> (1982); MO coordination; Atomic configuration: $Ac_{\alpha}c_{\beta}Bb_{\beta}c_{\gamma}Ab_{\alpha}byCb_{\beta}c_{\gamma}$. (b): Lowest energy structure determined by Yourdshahyan <i>et al.</i> (1999); MO coordination; Atomic configuration: $Ac_{\beta}b_{\gamma}Bc_{\alpha}c_{\gamma}Ab_{\gamma}c_{\beta}Cb_{\alpha}$.	112
Figure 5.12.	Powder XRD patterns generated from the optimised structure based on the potentials of Catlow <i>et al.</i> (1982) and the Ollivier <i>et al.</i> (1997) experimental results.	116
Figure 5.13.	Closer view of powder XRD patterns from Figure 5.13.	116
Figure 5.14.	Lowest energy stable structure determined using the potential parameters of Catlow <i>et al.</i> (1982) and after optimisation with DFT.	117
Figure 5.15.	Powder XRD patterns generated from the lowest energy stable structure optimised using DFT, and the Ollivier <i>et al.</i> (1997) experimental results.	118
Figure 6.1.	DTA-TGA results for Alcoa C31 gibbsite.	121
Figure 6.2.	Example XRD scans of calcination products from Alcoa C31 gibbsite calcined at 285 °C for eight hours, Alcoa C31 gibbsite calcined at 315 °C for six hours, and synthesised gibbsite calcined at 315 °C for six hours.	122
Figure 6.3.	Example XRD scan of boehmite. Prepared by hydrothermal treatment of synthesised gibbsite at 158 °C for 10 days.	122
Figure 6.4.	DTA-TGA results for hydrogenated boehmite and γ - Al_2O_3 sample resulting from the calcination of hydrogenated boehmite at 600 °C.	124
Figure 6.5.	Example XRD scans from heating trials to investigate the effect of milling and calcination time.	126
Figure 6.6.	Example difference plots from neutron diffraction data collected <i>in-situ</i> during calcination, of deuterated boehmite precursor.	128
Figure. 7.1.	Single-phase refinement plots for the models used, with internal parameters refined.	134
Figure 7.2.	Neutron diffraction data obtained from γ - Al_2O_3 prepared by <i>in situ</i> heating of deuterated boehmite precursor at 600 °C.	135
Figure 7.3.	Refinement plots for dual-phase refinements.	138

Figure 7.4.	MAS-NMR spectrum of γ -Al ₂ O ₃ prepared from hydrogenated boehmite precursor.	141
Figure 7.5.	Refinements for cubic models against neutron data obtained from deuterated boehmite heated <i>in situ</i> to form γ -Al ₂ O ₃ .	143
Figure 7.6.	Resulting profiles of the peak at $2\theta \sim 51^\circ$ generated by refinement of structure models.	144
Figure 7.7.	SAED patterns, with tetragonal, $I4_1/amd$, indexing diagrams.	145
Figure 7.8.	Rietveld refinement of the Tetragonal-8c model for γ -Al ₂ O ₃ prepared by heating <i>in situ</i> from deuterated boehmite precursors.	149
Figure 7.9.	Illustration of the procedure employed in the hydrogen refinement trials.	151
Figure 7.10.	Best fits for the refinement trials incorporating hydrogen in the structure of γ -Al ₂ O ₃ .	153
Figure 8.1.	Examples of grain shapes.	159
Figure 8.2.	Examples of microstructure.	160 161
Figure 8.3.	MAS-NMR spectra for γ -Al ₂ O ₃ prepared from hydrogenated boehmite precursor, calcined between 500 and 900 °C.	163
Figure 8.4.	XRD patterns for hydrogenated boehmite calcined between 500 and 900 °C.	164
Figure 8.5.	HRPD neutron diffraction patterns for hydrogenated boehmite pre-calcined for seven hours at temperatures between 500 and 900 °C.	164
Figure 8.6.	SAED patterns, looking down the [0k0] zone axis, for hydrogenated boehmite pre-calcined between 500 and 900 °C.	165
Figure 8.7.	Indexing diagrams, using the $I4_1/amd$ space group, looking down the [0k0] zone axis, for γ -Al ₂ O ₃ and γ' -Al ₂ O ₃ .	166
Figure 8.8.	Variation in a and c parameters for γ -Al ₂ O ₃ from Rietveld refinement of neutron diffraction data collected at room temperature.	169
Figure 8.9.	Variation in oxygen fractional y coordinate from Rietveld refinement of neutron diffraction data with calcination temperature for various samples.	170
Figure 8.10.	Variation in occupancy of octahedral (8c and 8d) and tetrahedral (4a) site positions from Rietveld refinement of neutron diffraction data with calcination temperature for various samples.	171

Figure 8.11.	Rietveld refinement for γ' -Al ₂ O ₃ formed by calcination of hydrogenated boehmite calcined at 800 °C for seven hours.	173
Figure 9.1.	Specific surface area measurements from BET and SAXS.	182
Figure 9.2.	The measurable intensities of the samples that have been calcined at different temperatures from SAXS.	182
Figure 9.3.	Porod plots of the measurable intensities.	183
Figure 9.4.	TEM images showing the lamellar porous microstructure.	185
Figure 9.5.	Mean pore diameter obtained from SAXS.	186
Figure 9.6.	Percentage of water contained within the bulk and at the surface of γ -Al ₂ O ₃ samples.	188
Figure 9.7.	Ignition-loss data represented as H/Al ratios compared with PGAA data of γ -Al ₂ O ₃ samples.	189
Figure 9.8.	Normalized NVS data collected after pre-drying to drive off surface water for boehmite calcined between 500 and 800 °C and bulk ice.	191
Figure 9.9.	Illustration of the difference between the NVS spectra of pre-dried and non-pre-dried (wet) samples of γ -Al ₂ O ₃ .	192
Figure 9.10.	DRIFT and transmission IR spectra collected after surface water was driven off for boehmite calcined between 500 and 900 °C.	194
Figure 9.11.	O-H/AlO ₆ , H-O-H/AlO ₆ , and AlO ₄ /AlO ₆ , ratios determined from transmission IR data.	195
Figure 10.1.	Examples of the oxygen sublattice, viewed down the <i>c</i> axis.	200
Figure 10.2.	Examples of neutron diffraction patterns simulated from just the oxygen sublattice.	200
Figure 10.3.	Key statistics for occupancy and energy distribution of structures obtained from the optimisation of the cubic <i>Fd$\bar{3}m$</i> and tetragonal <i>I4₁/amd</i> system structures with interatomic potentials.	202
Figure 10.4.	Occurrence of each type of site position throughout all optimised structures.	203
Figure 10.5.	Examples of diffraction patterns simulated from the <i>Fd$\bar{3}m$</i> system.	205
Figure 10.6.	Examples of diffraction patterns simulated from the <i>I4₁/amd</i> system.	206
Figure 10.7.	Typical experimentally measured neutron diffraction data obtained from γ -Al ₂ O ₃ prepared from highly-crystalline boehmite.	206

Figure 10.8.	Example from the $Fd\bar{3}m$ system of the improvement to the simulated structure provided by DFT calculation.	208
Figure 10.9.	Example diffraction patterns generated from the reproduced calculations of the Gutiérrez <i>et al.</i> (2002) and Sohlberg <i>et al.</i> (1999).	208
Figure 10.10.	Examples of diffraction patterns generated from c symmetry based starting structural configurations of the $Fd\bar{3}m$ system and $I4_1/amd$ system of structures.	210
Figure 10.11.	Examples of diffraction patterns of oxygen sublattice after optimisation using interatomic potentials and after optimisation with DFT.	212
Figure 10.12.	Key statistics from optimisations of c symmetry based structural configurations of the cubic $Fd\bar{3}m$ and tetragonal $I4_1/amd$ system structures with interatomic potentials.	213
Figure 10.13.	Examples of diffraction patterns simulated from c symmetry based structures of the $Fd\bar{3}m$ system.	217
Figure 10.14.	Examples of diffraction patterns simulated from c symmetry based structures of the $I4_1/amd$ system.	218
Figure 10.15.	Simulated diffraction patterns exhibiting the greatest difference from experiment for c symmetry based structures.	219
Figure 10.16.	Supercell structure based on $Fd\bar{3}m$ symmetry, with 10 cations on $8a$, 19 cations on $16c$, 30 cations on $16d$, and 5 cations on $48f$ site positions, after optimisation with interatomic potentials and DFT.	222
Figure 10.17.	Supercell structure based on $I4_1/amd$ symmetry, with 11 cations on $4a$, 1 cation on $4b$, 18 cations on $8c$, 30 cations on $8d$, 1 cation on $8e$, and 3 cations on $16g$ site positions, after optimisation with interatomic potentials and DFT.	222
Figure 10.18.	Illustration of (a): $Fd\bar{3}m$ system structure represented in Figure 10.16 and Table V, after optimisation of supercell using 4 k-points; (b): $I4_1/amd$ system structure represented in Figure 10.17 and Table VI, after optimisation of supercell using 2 k-points.	223

List of Tables

Table 2.1.	Examples of computational studies on the bulk structure of γ -Al ₂ O ₃ .	37
Table 4.1.	X-ray Diffractometer Specifications.	71
Table 4.2.	Potentials incorporated into the Buckingham Model for this study.	83
Table 5.1.	Summary of site positions available for occupation in the cubic, $Fd\bar{3}m$, and tetragonal, $I4_1/amd$, space groups used to describe the structure of γ -Al ₂ O ₃ .	91
Table 5.2.	Summary of the application of selection criteria to the total number of possible starting structures to obtain a reduced sample pool to be is optimised.	98
Table 5.3.	Summary of single point energies for the structures with the two lowest mean number of nearest neighbour cations.	98
Table 5.4.	Lattice Parameters for the κ -Al ₂ O ₃ structure.	112
Table 5.5.	Calculated atomic coordinates for the κ -Al ₂ O ₃ structure.	113
Table 5.6.	Al-O bond length data within the octahedra of the κ -Al ₂ O ₃ structure.	114
Table 5.7.	Calculated cell parameters and atomic coordinates for the κ -Al ₂ O ₃ structure using DFT.	118
Table 7.1.	Structure models used in preliminary Rietveld structure refinements.	132
Table 7.2.	Refinement results for previous study models. Results are shown for refinements where backgrounds were manually fixed.	134
Table 7.3.	Refinement results for present study models. Results are shown for refinements where backgrounds were manually fixed.	135
Table 7.4.	Results for dual-phase refinements. Results are shown for refinements where backgrounds were manually fixed.	137
Table 7.5.	Refinement results for cubic model fits against neutron data obtained from deuterated boehmite heated <i>in situ</i> to form γ -Al ₂ O ₃ . Results are shown for refinements where background functions were incorporated (Cheby I), in contrast to Tables 7.2 - 7.4 in section 7.1.2 where backgrounds were manually fixed.	143
Table 7.6.	Equivalent Miller indices for the cubic and tetragonal, $I4_1/amd$, representations of the structure of γ -Al ₂ O ₃ .	146

Table 7.7.	Refinement results for the Tetragonal-8c model of γ -Al ₂ O ₃ from the various precursors.	148
Table 7.8.	Structural parameters of boehmite derived γ -Al ₂ O ₃ .	148
Table 8.1a.	Structural parameters of γ' -Al ₂ O ₃ formed by calcination of hydrogenated boehmite calcined at 800 °C for seven hours.	175
Table 8.1b.	Aluminium – Oxygen bond lengths (Å) and angles (°) for γ' -Al ₂ O ₃ formed by calcination of hydrogenated boehmite calcined at 800 °C for seven hours.	176
Table 8.2a.	Structural parameters of γ' -Al ₂ O ₃ formed by calcination of hydrogenated boehmite calcined at 900 °C for seven hours.	177
Table 8.2b.	Aluminium – Oxygen bond lengths (Å) and angles (°) for γ' -Al ₂ O ₃ formed by calcination of hydrogenated boehmite calcined at 900 °C for seven hours.	178
Table 9.1.	Calculated contribution of the surface to the total volume.	187
Table 10.1	Summary of the distribution of cations among the possible site positions for all 513 optimised structures of each symmetry system investigated.	215